# Enhanced Rate Capability of Polymer-Derived SiCN Anode Material for Electrochemical Storage of Lithium with 3-D Carbon Nanotube Network Dispersed in Nanoscale Postprint

**Authors:** Zhang, JW, Xu, CH, Liu, ZP, Wang, W, Xin, X, Shen, L, Zhou, XB, Zhou, J, Huang, Q

**Date:** 2017-04-06T00:00:00+00:00

## Abstract

Electrochemical performances of multi-walled carbon nanotubes (CNT)-SiCN composite have been investigated. The sample was synthesized by a simple ultrasonication assisted method combined with high-temperature pyrolysis and characterized by Fourier transfo

## Full Text

### Enhanced Rate Capability of Polymer-Derived SiCN Anode Material for Electrochemical Storage of Lithium with 3-D Carbon Nanotube Network Dispersed in Nanoscale

**Junwei Zhang[1],[3], Caihong Xu[2], Zhaoping Liu[1], Wei Wang[1], Xing Xin[1],[3], Lu Shen[1],[3], Xiaobing Zhou[1], Jie Zhou[1], and Qing Huang[1],∗**

[1]Ningbo Institute of Material Technology and Engineering, Chinese Academy of Sciences, Ningbo 315201, China
[2]Beijing National Laboratory for Molecular Science (BNLMS), Institute of Chemistry, Chinese Academy of Sciences, Beijing 100190, China
[3]Graduate School of Chinese Academy of Sciences, Beijing 100039, China

The electrochemical performances of multi-walled carbon nanotube (CNT)-SiCN composites have been investigated. The samples were synthesized by a simple ultrasonication-assisted method combined with high-temperature pyrolysis and characterized by Fourier transform infrared spectroscopy, Raman spectroscopy, X-ray diffraction, field emission scanning electron microscopy, and transmission electron microscopy. In this composite, CNTs were uniformly

distributed in the SiCN ceramic matrix, retained structural integrity during the polymer-ceramic conversion, and formed relatively strong bonding with the SiCN ceramic matrix. When tested as an anode in a half-cell configuration, the obtained composite exhibited enhanced rate capability and cyclic capacity compared to pristine SiCN powder, CNTs, and graphite. It could deliver a capacity of 222.7 mA h/g when charged at 2000 mA/g, while the SiCN anode showed nearly no capacity even at a low current density of 200 mA/g. It is expected that the CNT-SiCN composite, and perhaps the broader series of CNT-PDC composites, may be prospective candidates for high-power applications.

**Keywords:** Polymer-Derived Ceramic, Carbon Nanotube, Silicon Carbonitride, Electrical Conductivity, Lithium Ion Batteries, amorphous polymer-derived

## 1. INTRODUCTION

Silicon-based polymer-derived ceramics (PDCs), such as silicon carbonitride (SiCN) and silicon oxycarbide (SiCO), have recently attracted increasing attention for potential application as anode materials in lithium-ion batteries (LIBs) [**?**]. PDCs exhibit numerous advantageous properties for this application. They are covalently bonded ceramics, which makes them chemically inert with respect to battery components and lightweight. Furthermore, their chemical and physical properties can be tailored by varying the starting polymer compositions. The finely dispersed $sp^2$-hybridized disordered carbon within the amorphous covalently bonded network of PDCs forms either a 3-dimensional percolating cage-like structure or isolated carbon clusters in carbon-rich and carbon-poor PDC-based ceramics [**?**, **?**]. This disordered carbon can not only provide abundant effective Li storage active sites but also offer electrical conducting paths throughout the material [**?**]. Meanwhile, the interconnected nanopores (~0.5 nm in diameter, a size much larger than that of Li ions (0.076 nm) [**?**, **?**]) and the so-called mixed bond configurations of the amorphous ceramic network (tetrahedrally coordinated silicon, i.e., SiCxOyNz, where x + y + z = 4) contained in the loose network of PDCs primarily serve to provide smooth paths for rapid Li ion transfer [**?**, **?**], with a secondary role as intercalation sites for Li ions.

Despite these advantages, most commercially used PDCs with high Li ion intercalation capacity have electrical conductivity between that of semiconductors (e.g., SiC) and insulators (e.g., silicon nitride). This means substantial internal resistance forms between PDC particles and the current collector, and large volume changes also occur during high current density, rapid charging and discharging (high-rate) cycling. Under these conditions, electrochemical oxidation and reduction reactions during high-rate cycling are restricted mainly to the outer surfaces of the PDC particles, ultimately resulting in much lower capacity and poorer cyclic performance accompanied by anode structure pulverization. Thus, poor electrical conductivity represents the main bottleneck restricting PDC applications in high-power and energy-density fields.

Therefore, once the structure of PDCs is determined, it is reasonable to infer that internal resistance would be significantly diminished and higher utilization of active regions in PDCs would be achieved if the electrical conductivity of PDCs were substantially improved, potentially enabling much higher capability and better cyclic performance for high-rate applications.

To date, studies on PDC anode materials have mainly focused on improving capacity and cyclic capability at relatively low current densities (less than 50 mA/g), with only a few investigating high-rate performance. Even less attention has been paid directly to investigating the relationship between the electrical conductivity of PDCs and high-rate performance [**?**]. Although good results were achieved, these studies actually focused on finding methods to increase the number of active sites or improve intimate contact between PDC particles and the current collector [**?**, **?**]. These approaches can be divided into several categories: (a) using carbon-rich pre-ceramic Si-polymers [**?**]; (b) addition of carbon or carbon precursors to Si-polymers, such as SiCN-graphite [**?**], graphene nanosheets-SiOC [**?**], CNT-based core-shell composites, nanowires, or paper [**?**], and hard carbon (potato starch) [**?**]; (c) modification through heat treatments [**?**, **?**]; (d) elemental doping of boron [**?**, **?**]; and (e) improving intimate contact between PDC anode particles and the current collector [**?**, **?**]. While positive effects were achieved using these methods, approaches using carbon-rich pre-ceramic Si-polymers and addition of carbon or carbon precursors could improve electrical conductivity while also increasing total active sites in PDC-based anodes to a large extent, as seen in CNT-based core-shell composites, which complicates the actual mechanisms linking PDC electrical conductivity and high-rate performance.

Moreover, to build a 3-dimensional connected conductive network, the volume fractions of graphite, graphene, or potato starch added in 2- or 3-dimensional forms might be so high that the superior and stable structure of PDC would be destroyed, adversely resulting in rather low electrochemical performance compared to pristine PDC anodes [**?**]. Meanwhile, modification through heat treatments and elemental doping of boron showed limited effects due to relatively low electrical conductivity ($8.7 \times 10^{-4}$ S/cm) [**?**, **?**, **?**]. Therefore, it is necessary to construct a simple architecture to investigate the effect of electrical conductivity on the high-rate performance of PDC anodes.

To investigate this effect, we propose a strategy of building a 3-dimensional conductive network throughout the PDC particle matrix using a secondary phase. For this strategy, the secondary phase should meet three requirements: (i) excellent electrical conductivity and low electrochemical activity with Li ions; (ii) chemical inertness with PDC during pyrolysis; and (iii) the volume fraction added should be as low as possible. CNTs are an appropriate candidate.

In most studies, the major role of CNTs is as a conductive agent due to their relatively low capacity and cycling ability [**?**]. Compared with graphene, graphite, or hard carbon with 2- or 3-dimensional morphology, CNTs with 1-dimensional form are more conducive to building a 3-dimensional conductive network. Ad-

ditionally, CNTs distributed in the PDC matrix will not affect the isotropic insertion of Li ions into active sites in the PDC matrix. Moreover, considering that multi-walled carbon nanotubes have demonstrated better performance in Li-ion batteries compared with single- or double-walled CNTs [**?**] and that carbon thermal reduction could occur between CNTs and SiCO ceramic [**?**], we selected multi-walled carbon nanotubes as the conductive agent and a relatively low disordered carbon-containing SiCN ceramic as the PDC matrix, with a CNT mass fraction of 10 wt.% in SiCN. In the CNT-SiCN composite synthesized in this study, CNTs exhibited homogeneous distribution throughout the SiCN matrix.

## 2.1. Preparation of Composite

Polysilazane liquid (-[$NHCH_3Si(CH_3)NH$] -[$CH_3Si(H)NH$] -) [**?**], which can be thermally pyrolyzed to form amorphous SiCN, was used as the starting material. In a typical synthesis, 0.1 g of multi-walled carbon nanotubes (CNTs) (Shenzhen Nanotech Port, China) was dispersed in $1.0 \times 10^4$ mL of N,N-dimethylformamide (DMF, Aladdin, GC grade) that had been refluxed with sodium wires for 24 h to remove residual water and other hydroxyl group-containing compounds. The mixture was then sonicated and magnetically stirred for 45 min to eliminate unwanted agglomerations. The CNT-DMF dispersion was mixed with 1.125 g of polysilazane. After stirring for 0.5 h, the mixture underwent decompression distillation at approximately 55 °C for 3 h to remove DMF. The obtained mixture was held in the decompression distillation unit and heated to 200 °C for 2 h for precursor cross-linking, followed by pyrolysis at 1000 °C for 2 h under argon atmosphere with heating and cooling rates of 5 °C/min to yield the CNT-SiCN composite (Fig. 1). For comparison, SiCN powder was also synthesized as a blank sample following the same experimental procedures, except that 1.125 g of polysilazane was mixed with DMF without CNT dispersion. As the ceramic yield of polysilazane is approximately 80 wt.%, the CNT percentage in the final CNT-SiCN composite was determined to be 10 wt.%.

Scanning electron microscopy (SEM) imaging of cross-linked CNT-polysilazane and CNT-SiCN composite was performed using an SEM (Hitachi, S-4800). Transmission electron microscopy (TEM) was carried out using a 100 kV TEM (JEOL, 2100 HR). Fourier transform infrared (FT-IR) spectra were collected using a liquid nitrogen-cooled Thermo-Nicolet 6700 FT-IR spectrometer in diffuse reflectance mode. Crushed powder specimens were mixed with KBr powder prior to spectral collection. X-ray diffraction (XRD) was performed using a Bruker D8 Advance powder X-ray diffractometer operating at room temperature with Cu K$\alpha$ radiation and a nickel filter. Raman spectroscopy was also carried out to evaluate disordered carbon in the pyrolyzed specimens using a Renishaw inVia-reflex system equipped with an air-cooled CCD and an argon ion laser with a wavelength of 532 nm.

## 2.2. Preparation of the Electrodes and Cells

The obtained CNT-SiCN composite and SiCN powders were ground in a mortar and sieved to 48  m. The CNT-SiCN composite powders were mixed with acetylene black powder as a conductor and polytetrafluoroethylene as a binder at a weight ratio of 85:10:5. Ethanol was added to the mixture, which was then mechanically stirred to form a slurry. The slurry was spread on the rough side of a copper foil and rolled into a thin film during ethanol evaporation. The thin film was cut into disks (diameter: 9 mm) to form anodes fitting the size of coin-type batteries (CR2032). The electrode disk was assembled into a battery in a glove box using Celgard 2300 (Celgard, Charlotte, NC) as a separator, Li foil as counter and reference electrodes, and 1 mol/dm$^3$ $LiPF_6$ in ethylene carbonate, propylene carbonate, and dimethyl carbonate (1:1:1 by volume, Aladdin, Shanghai, China) as electrolyte.

The weight fraction of CNT-SiCN composite in the electrode was input into the measuring system (LAND battery testing system software 5.3B version). Galvanostatic charge-discharge cycle tests were performed on a battery testing system (LAND 2001A, Wuhan Jinnuo, China) at a current density of 100 mA $g^{-1}$ in the potential range of 0–3.5 V versus $Li^+/Li$. The discharge and charge capacities of the CNT-SiCN composite anode in absolute value (mA h) and weight-normalized value (mA h $g^{-1}$) were automatically generated by the measuring system. To understand the electrochemical performance of the CNT-SiCN composite anode, SiCN powders were used as a reference anode with electrochemical performance measured under identical conditions.

## 3. RESULTS AND DISCUSSION

SEM and TEM images of the CNT-SiCN composite are shown in Figure 2

. In Figures 2(a) and (b), CNTs are distributed homogeneously in the SiCN matrix and exhibit a 3-dimensional network-like distribution within SiCN particles (Fig. 2(e)). As shown in Figure 2(c), CNTs retained their original morphology during polymer-ceramic conversion. Residual holes or pits (point A) left by pulled-out CNTs in Figure 2(d) indicate relatively strong bonding between CNTs and the ceramic matrix, while pits (point B) from axially pulled-out CNTs reveal that this bonding is not exceptionally strong. In Figure 2(f), the surfaces of CNTs retained their integrity, and the selected area electron diffraction (SAED) pattern of the SiCN matrix shows that the amorphous nature of SiCN was unchanged by CNT introduction. These observations lead to the initial conclusion that both the added CNTs and SiCN matrix suffered no obvious chemical damage during polymer-ceramic conversion. All evidence indicates that CNT-SiCN composite with homogeneously distributed CNTs was successfully synthesized by a simple ultrasonication-assisted method combined with high-temperature pyrolysis. More interestingly, light-contrast linear regions (arrows in Fig. 2(f)) between CNTs and the SiCN matrix are clearly visible. These regions might be interconnected nanovoids attributed to differences in thermal expansion co-

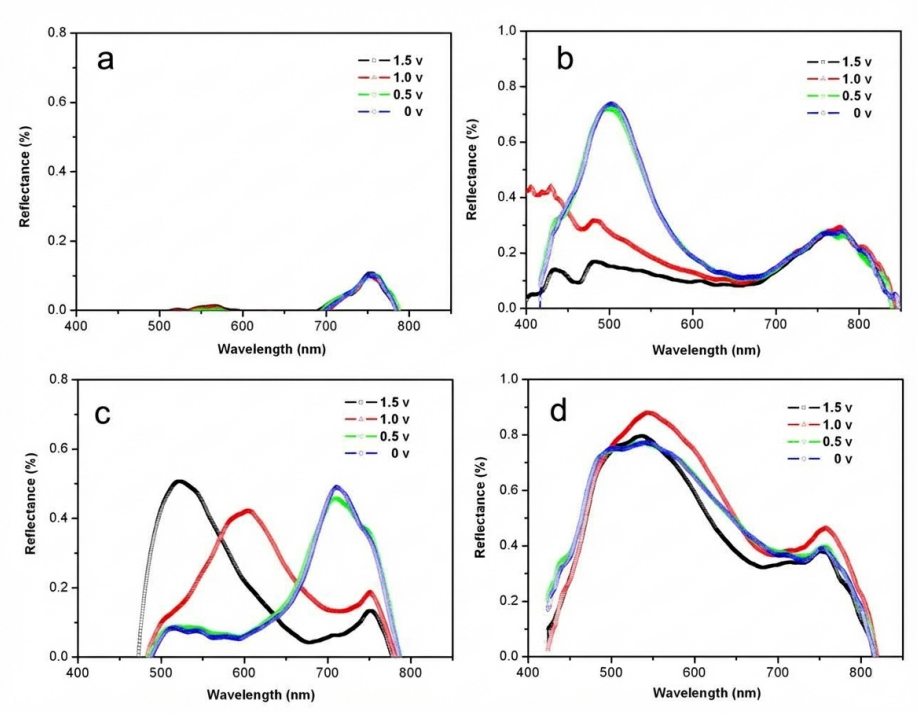


Figure 1: Figure 2

efficients between the two components or to decomposition/elimination of organic moieties (such as methyl, vinyl groups) and Si-H or Si-NH groups during polymer-ceramic conversion. These light-contrast linear regions could further promote rapid Li ion transfer during electrochemical discharging and charging processes. More recently, Ionescu et al. incorporated multi-walled carbon nanotubes within an insulating SiCN matrix by a mechanical milling method [**?**], where a polysilazane was pre-crosslinked, mixed with multi-walled CNTs, and subsequently warm-pressed and pyrolyzed in argon at 1100 °C. Upon adding 1 vol.% CNTs to SiCN, the AC conductivity increased by 7 orders of magnitude: the AC conductivity of SiCN was $10^{-9}$ S/cm, whereas the SiCN/multi-walled CNT nanocomposite containing 5 vol.% CNTs exhibited a conductivity of $7.6 \times 10^{-2}$ S/cm [**?**]. An et al. also showed that mechanical properties of SiCN-CNT composites were significantly improved by adding only 6.4 vol.% CNT [**?**]. As the density of CNTs (1.80 g/cm$^3$) used in this study is lower than that of amorphous SiCN (2.35 g/cm$^3$), it is reasonable to conclude that the CNT percentage added in this study could build a 3-dimensional conductive network throughout the SiCN matrix.

XRD patterns (Fig. 3 FIGURE:3) confirmed the amorphous nature of both the CNT-SiCN composite and SiCN pyrolyzed at 1000 °C for 2 h. Only a small diffraction peak at 2 = 26° belonging to the (002) plane of disordered carbon was detected. This peak is thought to derive from ordered stacking of ring-like structures along the c-axis of graphene layers in disordered carbon and disordered stacking along the a- or b-axis (i.e., (100) plane) of graphene layers, implying that the characteristic structure of disordered carbon is localized within the amorphous SiCN matrix. FT-IR spectra of crosslinked polysilazane and crosslinked CNT-polysilazane composite are similar to that of uncrosslinked liquid polysilazane (Fig. 3(b) and detailed information in Table I) [**?**, **?**]. Absorption peaks of C=C at 1593.2 cm$^{-1}$ and C-H at 3048.7 cm$^{-1}$ disappeared during crosslinking. Only a new absorption peak of Si-O-Si at 1042.1 cm$^{-1}$ with very weak intensity was detected, attributed to hydrolysis and oxidation of Si-N bonds during the experiment. These results imply that the pristine nature of polysilazane changed little during processing. Furthermore, because the CNT percentage in the crosslinked composite is low and even slightly lower than that in the final pyrolyzed composite (10 wt.%), no obvious absorption peak belonging to CNTs could be captured by FT-IR, and chemical interaction of polysilazane with CNT sidewalls could not be confirmed. However, based on this analysis, physical adhesion of polysilazane on CNT surfaces can be safely predicted.

Raman spectroscopy is a technique normally employed for characterizing carbon-containing materials. In this study, it was used to evaluate the disordered carbon phase localized in the SiCN matrix. Figure 3(c) displays Raman spectra of the CNT-SiCN composite and SiCN pyrolyzed at 1000 °C for 2 h. Both specimens show two typical features of disordered carbon: the D (disordered) band at ~1340 cm$^{-1}$ and the G (graphite) band at ~1600 cm$^{-1}$ [**?**, **?**]. The spectra show similar peak positions for each specimen. In Figure 3(c), a weak peak

(position slightly higher than 1600 $cm^{-1}$) belonging to $sp^3$ carbon could only be detected in the SiCN specimen, meaning the non-conductive $sp^3$ carbon phase disappeared upon CNT introduction into the SiCN matrix. The widened G band peak reveals that several graphene layers in the disordered carbon were stacked disorderly, while the widened and relatively strong D band signal further suggests that the disordered carbon is highly defective.

The Raman spectra were used to estimate the lateral cluster size (L ) of disordered carbon according to the equation reported by Ferrari and Robertson [**?**]: $I(D)/I(G) = C(\lambda)L^{2}$, where I(D) and I(G) are integrated intensities of the D and G bands, respectively; $\lambda$ is the laser line wavelength; and $C(\lambda)$ is a coefficient determined by $\lambda$. To obtain integrated intensities, Lorentzian curve fitting was performed [**?**, **?**]. The calculated I(D)/I(G) ratios for CNT-SiCN composite and SiCN specimens were 1.51 and 1.27, respectively. As accurate values for the laser line wavelength at 532 nm could not be found, the exact L value is difficult to determine, but the ratio of L for CNT-SiCN composite to SiCN was calculated as 1.09, implying that the size of disordered carbon clusters localized in the SiCN matrix becomes slightly larger when CNTs are introduced. This phenomenon is very interesting and agrees with results from Segatelli et al. [**?**], who reported that carbon nanotube introduction is beneficial for nucleation and growth of graphene layers in disordered carbon. We can therefore assume that the reversible capacity of the CNT-SiCN composite anode will be slightly higher than that of the SiCN anode, because the lateral cluster size of disordered carbon is proportional to the number of reversible active sites for Li ion intercalation [**?**].

Figure 4

(a) shows the first, second, and 30th cycle discharge-charge curves of anodes made from the 1000 °C-pyrolyzed CNT-SiCN composite and comparative SiCN, respectively. These data were obtained at a current density of 100 mA/g between voltage limits of 0.001 and 2 V. Discharge represents Li insertion into the composite anode, while charge represents the opposite process. For easier comparison, discharge/charge capacities and coulombic efficiency values for the first and 30th cycles are summarized in Table II. The CNT-SiCN composite anode offered a first discharge capacity of 597.5 mA h/g, of which 313.2 mA h/g was reversible, giving a first coulombic efficiency of 52.4%. After 30 cycles, as seen in Figure 4(b), it still retained a stable capacity of 325.7 mA h/g with a coulombic efficiency of 99.1%. Apparently, the CNT-SiCN composite anode exhibited much better specific capacity than the SiCN anode (reversible capacity of ~67.3 mA h/g), commercially used graphite anode (reversible capacity of ~70 mA h/g at 100 mA/g) [**?**], and CNTs alone [**?**].

For the first cycle of the SiCN anode, a sloping discharge potential plateau at ~10-50 mV in Figure 4(a) suggests Li-ion intercalation into pores of the SiCN network, mesopores, and defects belonging to carbon nanotubes. These discharge platforms disappeared in the second cycle, indicating that some Li ions or less-

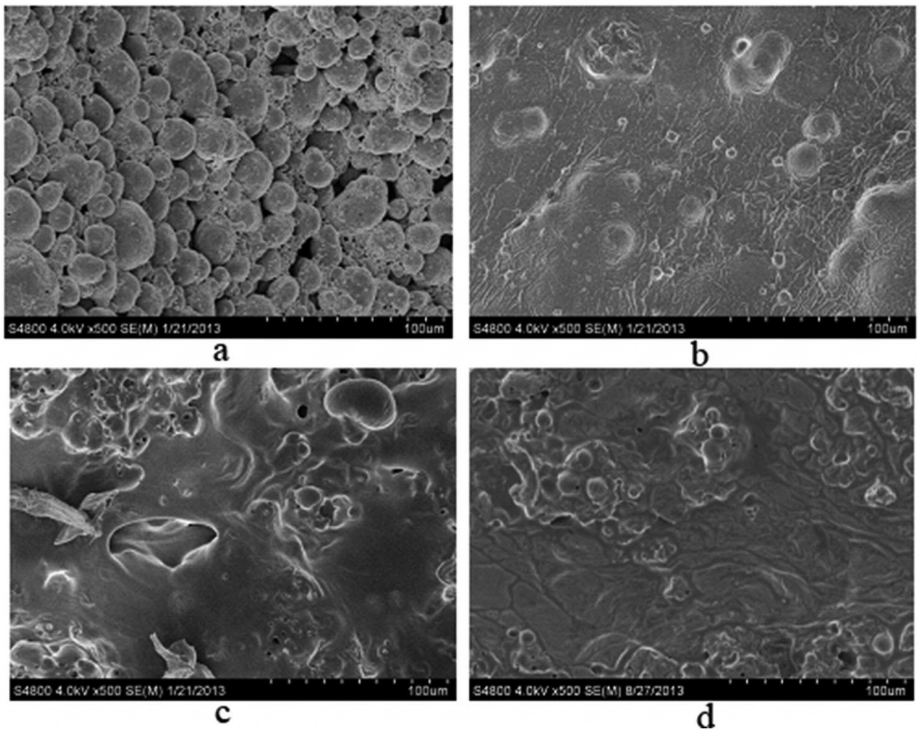


Figure 2: Figure 4

ionic Li atom clusters were trapped in pores, contributing to irreversible capacity. The electrochemical reactions occurring at the potential window between 0.8 V and 1.2 V in Figure 4(a) should be attributed to electrolyte decomposition and formation of a passivation layer (solid electrolyte interface, SEI) on SiCN particle surfaces. This process is responsible for the major part of irreversible capacity loss, but more importantly, this layer also protects against further reaction with electrolyte. Compared with SiCN anode discharge-charge curves, a platform starting at ~0.2 V suggests Li-ion intercalation between graphene nanosheets of isolated disordered carbon [**?**]. Fortunately, the CNT-SiCN composite anode exhibited a constant current (CC) charging stage at the electrochemical window between 50 mV and 1.0 V, where specific capacity changes proportionally with voltage, while the SiCN anode presented a constant voltage (CV) stage, meaning the SiCN anode could obtain most of its capacity only in the narrow potential region between 50 mV and 0.5 V. As is commonly understood for most electrodes, cells can be charged quickly by constant current in the former stage, while in the CV stage charging occurs slowly while maintaining potential at 0 V. Therefore, the CNT-SiCN composite anode is expected to show better high-rate performance than the SiCN anode due to its wider electrical potential margin. These results indicate it would be difficult for the SiCN anode to perform well in subsequent high-rate testing.

In general, tetrahedrally coordinated silicon containing oxygen (such as $SiC_3O$, $SiC_2O_2$, and $SiCO_3$) can sequester Li ions reversibly [**?**, **?**]; however, there was no $SiO_4$ unit in the CNT-SiCN composite or SiCN anode. The electrochemical capability of the CNT-SiCN composite should be attributed to the presence and amount of disordered carbon. Taking the upper value of 400 mA h/g as the reversible discharge capacity of CNTs in the composite anode [**?**], the contribution of CNTs to the CNT-SiCN composite capacity is calculated to be 40 mA h/g—only one-third of the reversible capacity (~325.7 mA h/g) obtained for the composite. Thus, many new active sites of disordered carbon were likely exploited with formation of the CNT conductive network throughout the SiCN matrix. Beyond higher reversible capacity, the higher coulombic efficiency in Figure 4(b) reveals that CNT introduction also results in better capacity retention during long-term cycling. It can therefore be reasonably deduced that the newly exploited active sites for reversible Li ion intercalation were mainly derived from isolated disordered carbon clusters originally localized in interior regions of the SiCN matrix, and that the SiCN anode could deliver its full capacity only when it had good electrical conductivity. In this case, when the CNT-SiCN composite was used as an anode, the CNT network could supply numerous paths for charge transfer from surface regions of SiCN particles to most isolated disordered carbon clusters distributed in interior regions of the SiCN matrix. Additionally, the slight increase in lateral cluster size of disordered carbon detected by Raman spectroscopy might also benefit the increase of reversible active sites in disordered carbon clusters.

Feng et al. also prepared SiCN-CNT composite anode material, but the carbon nanotubes they used were localized between SiCN particles and the copper foil,

acting as a conductive agent and flexible network to buffer volume expansion of SiCN particles [**?**]. Although they achieved higher capacity compared with SiCN and graphite anodes, the reversible capacity dropped gradually during the first 30 cycles [**?**]. We speculate the main reason is the poor cycling stability of carbon nanotubes when in direct contact with electrolytes, because CNTs tend to react continuously with electrolytes during discharging and charging. Consequently, as the thickness of the insulating SEI layer on CNT surfaces gradually increases, the electrical conductivity of the anode becomes progressively lower, leading to poor cyclic performance. In contrast, the CNT-SiCN composite synthesized in this study exhibited improved cyclic behavior, which could be attributed to complete protection of carbon nanotubes by the inert SiCN ceramic matrix.

Figure 4(a) also suggests significant hysteresis for both anodes during Li ion discharging-charging, and this hysteresis persisted during extended cycling. Such hysteresis likely results from differences in electrochemical potential of Li ions at the SiCN-electrolyte interface and the electrochemical potential of Li ions within the electrolyte that are in equilibrium with the lithium metal counter electrode.

Rate performance—capacity at increasing current density for Li extraction from the anode—was measured. Since rapid discharging capability is more important for full cells in high-rate applications, the discharge current density was kept constant at 100 mA/g while the charge current density was varied as shown in Figure 5 [FIGURE:5] (rate capacity of SiCN is not shown because it supplied nearly no capacity when charge current density reached 200 mA/g). The CNT-SiCN composite exhibited excellent rate capability: even at a charge current density of 2000 mA/g, it maintained an average capacity of 222.7 mA h/g. In contrast, SiCN showed no rate capability, which can be ascribed to the low electrical conductivity of the SiCN matrix. Compared with other work [**?**, **?**], the CNT-SiCN composite anode showed much higher rate capacity than graphite anodes (e.g., reversible capacity of ~70 mA h/g at 100 mA/g) [**?**]. The higher capacity of the CNT-SiCN composite during cycling is assumed to result mainly from two factors: superior electrical conductivity within CNT-SiCN composite particles and better electrical contacts between anode particle surfaces and the current collector, and good structural stability maintained by the 3-dimensional CNT network during Li ion intercalation/extraction. Consequently, new conducting paths formed, resulting in higher capacity values and excellent high-rate capability. Regarding the newly exploited active sites, these would be located in regions where conductive carbon nanotubes were centered, because reversible electrochemical reactions within anode particles are limited by the electrical conductivity of the SiCN matrix in which isolated disordered carbon clusters are encased.

These results are simply explained by the schematic in Figure 6 [FIGURE:6], which shows the most likely reason for the different electrochemical performance of the CNT-SiCN composite and SiCN anodes during high-current-density discharging. It is normal for charge capacity to decline at higher current densities,

which is dominated by electrical conductivity and Li ion diffusion coefficient. Once anode electrical conductivity is substantially improved, capacity may be further limited by kinetic diffusion processes of Li ions into SiCN particles or by reactions at conducting agent-SiCN-electrolyte triple junctions. Moreover, in addition to electrical conductivity contributions to high-rate capability, the light-contrast linear regions between CNTs and the SiCN matrix (Fig. 2(f)) may also provide numerous paths for rapid Li ion diffusion.

Singh et al. investigated the diffusion coefficient of Li ions in polymer-derived silicon oxycarbide-carbon nanotube composites with shell/core structure through galvanostatic intermittent titration technique (GITT) experiments, reporting that the diffusion coefficient of Li ions in Si(B)CN particles might increase simultaneously due to increased electrical conductivity in the shell/core composites [**?**, **?**]. Therefore, improvement in electrical conductivity might also be accompanied by a slight increase in the diffusion coefficient of Li ions in SiCN particles.

Based on these results, solutions should be found to meet commercial application needs for PDCs in high-power and energy Li-ion batteries. First, the electrical conductivity of PDCs should be high enough to provide conductive paths for electron transfer, and internal resistance should be minimized. Second, the effective diffusion distance for Li ions should be shortened to improve utilization of disordered carbon isolated in the PDC matrix and to reduce volume expansion of PDC anode particles during high-rate charging and discharging cycles. For the latter suggestion, synthesis of PDC particles in nano or porous forms [**?**] may be promising.

## 4. CONCLUSION

In this article, we present investigation of a new composite material with a 3-dimensional conductive network as an anode material for Li-ion batteries. This composite, composed of CNTs and amorphous polymer-derived SiCN, was synthesized by a simple ultrasonication-assisted method combined with high-temperature pyrolysis. In this composite, CNTs exhibited homogeneous distribution in the SiCN ceramic matrix, retained structural integrity during polymer-ceramic conversion, and formed relatively strong bonding with the SiCN ceramic matrix.

Regarding Li ion insertion/extraction, the CNT-SiCN composite exhibited higher capacity than the sum of both components. The outstanding electrochemical properties of the composite should be attributed to introduction of the superior conductive CNT network. CNTs supplied more paths for electrical contact, enabling charge transfer to isolated disordered carbon clusters formed within the polymer-derived SiCN ceramic matrix. Moreover, due to the high strength and toughness of carbon nanotubes, the new composite exhibited extraordinary stability during high-current-density cycling. In the obtained half-cell, the composite anode could deliver a capacity of 222.7 mA h/g when

charged at 2000 mA/g, while the SiCN anode showed nearly no capacity even at the low current density of 200 mA/g. In conclusion, CNT-SiCN composites, and perhaps the broader series of CNT-PDC composites, are interesting "high-power" anode materials for future high-power lithium-ion batteries, such as portable power suppliers and electric vehicles.

**Acknowledgment:** This work was financially supported by the National Natural Science Foundation of China (Grant No. 51172248), Zhejiang Provincial Natural Science Foundation of China (R12E020005), the 'Qianjiang Talent' program (2011R10020), and the International S&T Cooperation Program of China (2012DFA40550).

**References and Notes**

1. L. M. Reinold, M. Graczyk-Zajac, Y. Gao, G. Mera, and R. Riedel, J. Power Sources 236, 224 (2013).
2. R. Bhandavat, Z. J. Pei, and G. Singh, Nanomater. Energy 1, 324 (2012).
3. X. Liu, K. Xie, C. M. Zheng, J. Wang, and Z. Q. Jing, J. Power Sources 214, 119 (2012).
4. G. Mera, A. Tamayo, H. Nguyen, S. Sen, and R. Riedel, J. Am. Ceram. Soc. 93, 1169 (2010).
5. D. Su, Y. L. Li, Y. Feng, and J. Jin, J. Am. Ceram. Soc. 92, 2962 (2009).
6. J. Kaspar, G. Mera, A. P. Nowak, M. Graczyk-Zajac, and R. Riedel, Electrochim. Acta 56, 174 (2010).
7. H. Fukui, H. Ohsuka, T. Hino, and K. Kanamura, J. Power Sources 196, 371 (2011).
8. Y. Feng, G. X. Du, X. J. Zhao, and E. C. Yang, J. Appl. Electrochem. 41, 999 (2011).
9. P. A. Ramakrishnan, Y. T. Wang, D. Balzar, L. N. An, C. Haluschka, R. Riedel, and A. M. Hermann, Appl. Phys. Lett. 78, 3076 (2001).
10. A. M. Hermann, Y. T. Wang, P. A. Ramakrishnan, D. Balzar, L. N. An, C. Haluschka, and R. Riedel, J. Am. Ceram. Soc. 84, 2260 (2001).
11. L. F. Hu, M. S. Li, C. H. Xu, Y. M. Luo, and Y. C. Zhou, Surf. Coat. Technol. 203, 3338 (2009).
12. Z. B. Zhang, F. Zeng, J. J. Han, Y. M. Luo, and C. H. Xu, J. Mater. Sci. 46, 5940 (2011).
13. J. Luo, Z. B. Zhang, W. Liu, X. J. Wang, Z. J. Peng, Y. M. Luo, and C. H. Xu, J. Appl. Polym. Sci. 126, 853 (2012).
14. M. Graczyk-Zajac, C. Fasel, and R. Riedel, J. Power Sources 196, 6412 (2011).
15. J. Q. Wu, Y. M. Li, L. M. Chen, Z. B. Zhang, D. Wang, and C. H. Xu, J. Mater. Chem. 22, 6542 (2012).
16. G. T. Wu, C. S. Wang, X. B. Zhang, H. S. Yang, Z. F. Qi, P. M. He, and W. Z. Li, J. Electrochem. Soc. 146, 1696 (1999).
17. C. Garau, A. Frontera, D. Quiñonero, A. Costa, P. Ballester, and P. M. Deyà, Chem. Phys. 297, 85 (2004).
18. A. Varzi, C. Täubert, M. Wohlfahrt-Mehrens, M. Kreis, and W. Schütz,

J. Power Sources 196, 3303 (2011).
19. M. G. Segatelli, E. Radovanovic, A. T. N. Pires, M. d. C. Gonçalves, and I. V. P. Yoshida, Mater. Chem. Phys. 124, 1216 (2010).
20. L. N. An, W. X. Xu, S. Rajagopalan, C. M. Wang, H. Wang, Y. Fan, L. G. Zhang, D. P. Jiang, J. Kapat, L. Chow, B. H. Guo, J. Liang, and R. Vaidyanathan, Adv. Mater. 16, 2036 (2004).
21. E. Frackowiak, S. Gautier, H. Gaucher, S. Bonnamy, and F. Beguin, Carbon 37, 61 (1999).
22. H. Yamada, Y. Watanabe, I. Moriguchi, and T. Kudo, Solid State Ionics 17, 1706 (2008).
23. X. Liu, M. C. Zheng, and Kai Xie, J. Power Sources 196, 10667 (2011).
24. J. Electrochem. Soc. 152, A474 (2005).
25. J. Power Sources 112, 216 (2002).
26. Energy Environ. Sci. 2, 638 (2009).
27. J. Mater. Chem. 19, 9063 (2009).
28. J. Eur. Ceram. Soc. 28, 2247 (2008).
29. J. Power Sources 244, 80 (2013).
30. J. Mater. Chem. 22, 6542 (2012).
31. J. Power Sources 196, 3303 (2011).
32. J. Appl. Electrochem. 41, 999 (2011).
33. J. Am. Ceram. Soc. 92, 2962 (2009).
34. J. Power Sources 236, 224 (2013).
35. J. Power Sources 214, 119 (2012).
36. J. Am. Ceram. Soc. 93, 1169 (2010).
37. Electrochim. Acta 56, 174 (2010).
38. J. Power Sources 196, 371 (2011).
39. J. Mater. Sci. 46, 5940 (2011).
40. J. Appl. Polym. Sci. 126, 853 (2012).
41. J. Mater. Chem. 22, 6542 (2012).
42. J. Power Sources 196, 6412 (2011).
43. J. Mater. Chem. 19, 9063 (2009).

Received: 16 August 2013. Accepted: 26 January 2014.